Experimental and Numerical Investigation on Tsunami Run-up Flow in the Built Environment

Hidenori Ishii [a], Tomoyuki Takabatake [a]*, Miguel Esteban [a], Jacob Stolle [b], Tomoya Shibayama [a]

[a] *Department of Civil and Environmental Engineering, Waseda University, Tokyo, Japan*

[b] *Centre Eau Terre Environnement, Institut national de la recherche scientifique, Québec, Québec*

*E-mail address: takabatake@aoni.waseda.jp (Tomoyuki Takabatake, Corresponding author)

Experimental and Numerical Investigation on Tsunami Run-up Flow in the Built Environment

Abstract: Inland tsunami flows can be greatly affected by the presence of coastal buildings. The present study experimentally and numerically investigated the effects of nine different building layouts on 1) the tsunami inundation process and spatial velocity distribution, 2) the flow depth and velocity at a specific point, and 3) the extent of the area where shielding effects take place. High-speed video footage, PIV analysis, and the time history of flow depth, velocity, and momentum flux demonstrated significant differences in the tsunami run-up behaviour among the different building layouts considered. However, it was also shown that a decrease in the flow velocity always appears in front of and immediately behind the building(s), regardless of their layouts. The OpenFOAM simulations performed revealed that significant shielding effects appear in the leeside of the building. These findings can be used when considering where to place evacuation buildings, as constructing them directly behind another study structure could reduce construction costs and increase their stability. The obtained results were also applied to partially validate the method for calculating the channeling effects of tsunami loads provided in ASCE 7-16.

Keywords: tsunami; built environment; hydraulic experiment; inundation; OpenFOAM

1. Introduction

A tsunami can cause massive damage to coastal communities, as shown by recent events such as the *2004 Indian Ocean Earthquake Tsunami*, the *2011 Tohoku Earthquake and Tsunami*, the *2018 Palu Tsunami* and the *2018 Sunda Strait Tsunami* (see Synolakis and Bernard, 2006; Mori et al., 2011; Harnantyari et al., 2020; Takabatake et al., 2019, respectively). To prevent the loss of lives and property from such hazards, it is imperative to understand the nature of tsunami flow as it propagates overland.

This inland tsunami flow can be greatly affected by the presence of buildings or other structures. Although many common structures (such as residential housing, warehouses) can be destroyed due to the overland flow, reinforced concrete structures can often withstand the pressures exerted on them. As a result of the presence of such buildings, the flow of the tsunami changes locally, causing channelling and shielding effects due to flow constriction and obstruction, respectively. Such local flow effects were observed during the *2011 Tohoku Earthquake and Tsunami*, where Kakinuma et al. (2011) reported that a large reinforced concrete building, located in Onagawa Town, Miyagi Prefecture, Japan provided shielding effects for buildings behind it. Kakinuma et al. (2011) also pointed out that when the tsunami passed between two concrete buildings the velocity of the flow accelerated, resulting in significant local scouring between them. According to the NILIM (National Institute for Land and Infrastructure Management) and BRI (Building Research Institute) (2011), some wooden houses located behind a sturdy building remained standing due to the effects of shielding.

Extensive numerical and experimental research has been performed examining the interaction between tsunami-like waves and the built environment. Simamora et al. (2007) compared the effects of six different building layouts on tsunami loading. They indicated that when a structure is shielded by another structure, the tsunami force is reduced and, the closer the shielded building is to the seaward structure, the greater the effect. Oda et al. (2008) and Okamoto et al. (2009) investigated the reduction effects of multiple sturdy buildings on tsunami run-up distance, velocity, and flow depth. In the experiments of Nouri et al. (2010), dam-break waves were used to investigate the tsunami load on a free-standing structure, showing that flow constriction due to the presence of upstream obstacles increased impact forces exerted on a downstream structure. Goseberg (2013) experimentally investigated the reduction effects on maximum tsunami run-up distance when four different obstacle configurations aligned or staggered with rotation or non-rotation. Goseberg and Schlurmann (2014) focused on the features of the tsunami flow around one and two buildings placed parallel to the shoreline. Using Particle Image Velocimetry (PIV), the wake angles behind the buildings were shown to increase linearly as the generated tsunami propagated inland. Nakamura et al. (2014) numerically simulated tsunami forces on a structure when other similar ones were around it. Thomas et al. (2015) used a piston-type wavemaker to generate long-period waves in a wave basin and evaluated the effects of multiple configurations of obstacles on shoreward specimens. Their results demonstrated that the forces exerted on the specimen increased as the distance between the pair of seaward obstacles grew, but then decreased when the gap became too wide. Tomiczek et al. (2016) experimentally measured the pressure acting on a structure by varying the incident tsunami waves and onshore structure configurations, observing a reduction in pressure (40-70%) under various wave breaking conditions. Okumura et al. (2019) focused on the effects of the position of two buildings, and numerically investigated the change in tsunami overturning moment according to their layouts. Winter et al. (2020) experimentally investigated the effects of neighbouring structures on the resulting flow, pressure, and force on the structure. They reported that the shielded structure generally experienced weaker forces, while the applied pressure was higher in some locations, increasing the risk to some structural elements.

Some researchers have investigated the characteristics of tsunamis flowing through more realistic coastal city layouts. Cox et al. (2008) conducted physical experiments examining the impact of a tsunami on Seaside, Oregon, U.S.A. Prasetyo et al. (2019) constructed a 1:250 scale of Onagawa Town, Miyagi Prefecture, Japan, and investigated the inundation behaviour using two different tsunami-like waves. The experiments of Cox et al. (2008) were later numerically reproduced by Park et al. (2013), and Qin et al. (2018a, 2018b). Qin et al. (2018b) modelled a tsunami inundation process using both a depth-integrated 2D model (GeoClow) based on the nonlinear shallow water equations and a 3D model (OpenFOAM) based on the Reynolds-averaged Navier-Stokes equation. The results demonstrated that the three-dimensional (3D) model was able to simulate the flow characteristics more accurately, though these authors also highlighted the associated computational cost of the 3D model. Using a coastal community impacted by the *2012 Hurricane Sandy* as a case study area, Hatzikyriakou and Lin (2017) investigated the effects of the interaction between residential structures under an extreme hydrodynamic condition (in this case storm surge). These authors demonstrated that structures located seaward strongly influence the performance of other inland structures and suggested that hardening oceanfront structures could result in enhancing the overall resilience of the community.

The above studies have provided valuable knowledge that has increased the understanding of the interaction between tsunami inland flow and the built environment. While many studies have indicated that the shielding effect, which significantly reduces tsunami loads on a structure landward of another one, can be important (Kakinuma et al. 2011; Tomiczek et al. 2017; Robertson and Mohamed 2009; Winter et al., 2020; Wüthrich et al, 2018), limited studies have clarified the extent of the area where the shielding effect can work effectively. Thus, it is important to understand further how the spatial distribution of tsunamis flowing through various building configurations changes over time using the PIV technique. To further address these issues, a 3D study was developed at the Waseda University Tsunami Wave Basin, complemented by a 3D numerical model developed in OpenFOAM

The study presented here will build upon and compare to the results of previous studies outlined above. The main objectives of this study are:

1) Qualitatively and quantitatively describe the flow patterns around a range of building arrangements.
2) Investigate the influence of the building arrangement on the momentum flux on the leeside of the structures.
3) Determine the areal extent of the shielding as well as governing parameters.

2. Experimental Analysis

2.1 Experimental setup

Experiments were conducted at the Tsunami Wave Basin of Waseda University in Tokyo, Japan (width 4.0 m, length 9.0 m, height 0.5 m). A 2 m long stainless steel slope with an angle of 1/10, representing a typical shoreline along the Japanese Pacific coastline (Stolle et al., 2019), followed by a 2 m long stainless steel horizontal floor, was installed 4 m away from a wave maker at the edge of the basin (**Figure 1**). In all experimental conditions, the initial water level was kept 0.20 m from the bottom of the basin. In the experiments, a tsunami-like wave was generated from a vertical reservoir at the end of the basin. Before each experimental test, water was stored in the reservoir by a suction pump. Next, the air valves at the top of the reservoir were opened, releasing the stored water and creating a tsunami-like wave.

To investigate the tsunami inland flow around the building models, an area with a length of 0.8 m and a width of 0.7 m was set as the target for PIV analysis. To improve the accuracy of this PIV analysis, the floor of the target area was covered with a vinyl chloride plate and painted with oil paint (to suppress light reflection). The edge of the target area was defined as the origin of the x and z axes, and its centreline was defined as the origin of the y-axis (see **Figure 1**).

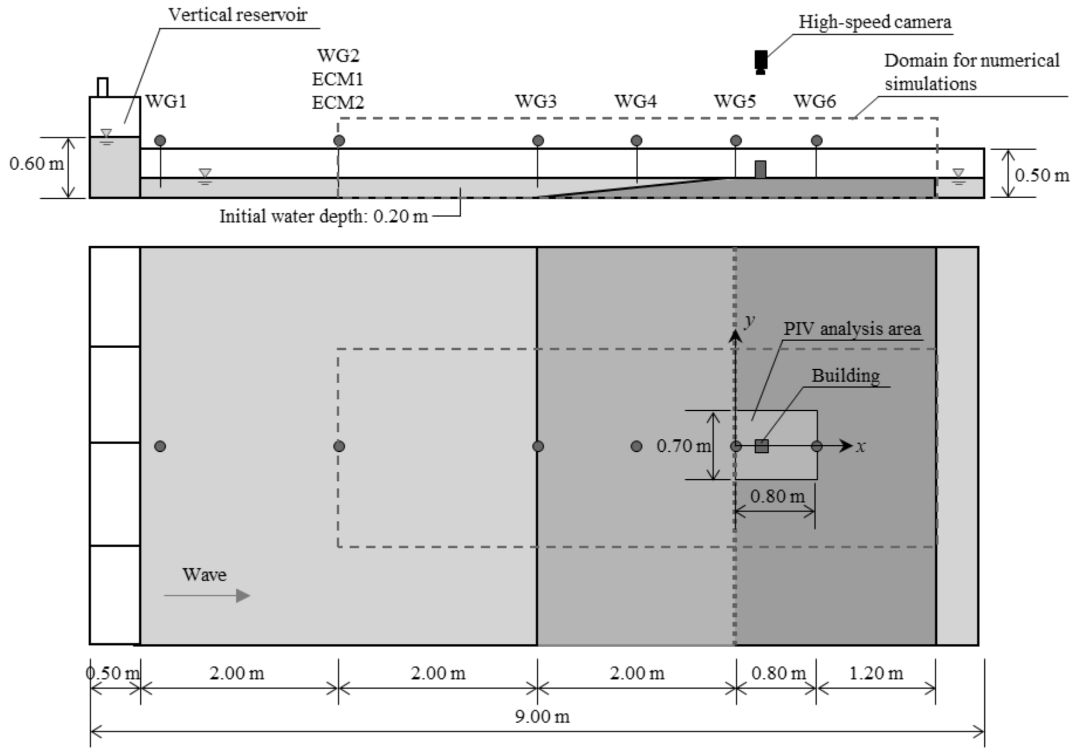

Figure 1 Schematic diagram of the tsunami wave basin. Small circles represent wave gauges and electromagnetic current meters. The dashed rectangular area corresponds to the domain range used for the numerical simulation (as detailed later).

A total of six capacitance-type wave gauges, WGs (CHT6-30/40, manufactured by KENEK Co. Ltd.), were used to record the water surface elevations. Four of them were installed in the offshore area and two were installed onshore (see **Figure 1**). A reference point was arbitrarily set at x = 0.80 m, and y = 0.0 m, which is at the same position as WG6. Time histories of the flow depth and velocity recorded at this point will be discussed later. Two electromagnetic current meters, ECMs (VMT2-200-04P/04PL, manufactured by KENEK Co. Ltd.) were also installed at the same position as WG2 to measure the flow velocity at a height of 0.15 m (ECM1) and 0.10 m (ECM2) from the bottom.

A high-speed camera (K4, manufactured by KATO KOKEN Co. Ltd. with a 1024 pixel (px) × 1024 px resolution) was mounted above the basin and used to measure the change in the spatial distribution of the velocity. In order to capture the water movement around the structure, styrene beads (particle size between 0.3 and 0.6 cm) were evenly distributed over the sea area before generating a tsunami-like wave. The captured images were later analyzed using a high-performance fluid analysis software (FlowExpert2D2C, KATO KOKEN Co. Ltd.), and converted to the plane flow velocity. In the analysis, particles having higher luminance were first selected inside the interrogation area (which was set to be 0.02 m $\times$0.02 m), and tracked in the next image using a search window having 0.15 m in x direction (flow direction) and 0.05 m in y direction. Through the procedure, the velocities in the analysis area (see **Figure 1**) could be obtained. Velocity at the position of WG6 was also obtained from the video image associated with PIV analysis. The sampling frequency of all the instruments was set to be 200 Hz.

The recordings of the high-speed camera were synchronized with the recording of WGs and ECMs using an LED light. The LED light was placed inside the view of the high-speed camera and connected to the Data Acquisition System, DAS (ADS2016, KENEK Co. Ltd.) used for recording WGs and ECMs. When the LED light turned on, the glowing light bulb was recorded by the high-speed camera and the change in voltage in the WGs was also recorded by DAS, which allows the data to be synchronized to within 0.01 s (Stolle et al. 2018; Iimura et al. 2020).

2.2 Experimental protocol

Rectangular wooden prisms (0.10 m length, 0.10 m width, 0.20 m height) were used to represent the obstacles (buildings). The size of the buildings was determined by considering the range of view of the high-speed camera and the typical size of a residential building in Japan. The experiments were performed at a scale of 1:80. The edges of the models were covered with vinyl chloride tape to make their surface roughness similar to that of the surface slope. The seaward distance between the shoreline and the building(s) was set to 0.20 m. Three different layouts were tested: a single building, two buildings aligned parallel to the shoreline, and two buildings aligned perpendicular to the shoreline (see **Figure 2**). A case without buildings was also tested, in order to observe the unhindered progress of the wave over land. For the parallel and perpendicular layout cases, the gap width varied from 0.05 to 0.30 m (at 5 cm interval increments). Thus, a total of nine building layouts were considered (see **Table 1**).

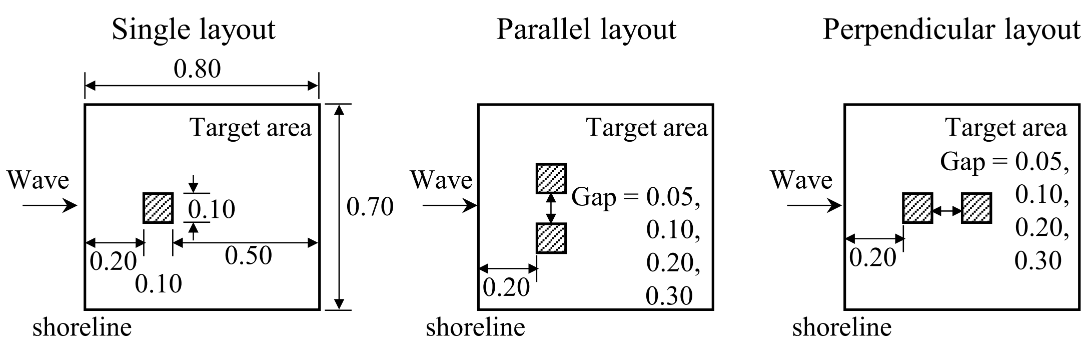

Figure 2 Building layouts used in the experiments (units: m). The rectangle area shown (length of 0.80 m and a width of 0.70 m) indicates the target area used for the PIV analysis (see **Figure 1**).

Table 1 Experimental protocol. The experimental categories are named to represent the initial conditions.

Experimental category	Layout	Gap (m)
N0	No buildings	-
S0	Single	-
PA05	Parallel	0.05
PA10	Parallel	0.10
PA20	Parallel	0.20
PA30	Parallel	0.30
PE05	Perpendicular	0.05
PE10	Perpendicular	0.10
PE20	Perpendicular	0.20
PE30	Perpendicular	0.30

The blockage ratio ($BR = 1 - W_c/W$) was used to define the structures with a parallel layout using the definition from the ASCE 7 Chapter 6 (ASCE, 2016), which defines the width of the channel between the outermost extent of the structures and the width of the structures as the exposed area of the structure.

The authors first repeated the case where no buildings were present or there was only one (single layout) five times, and confirmed that that the maximum values of water level and flow velocity recorded at each run were always within a 5% difference from the averaged value over all runs. After this, all other cases were repeated only three times. After confirming that the differences in values among the three runs were minimal for the recorded time histories of WGs and ECMs, the authors decided to use the results of the first run of each case for the subsequent analysis. However, the results having the largest value of the Luminance correlation coefficient among each run were used for the PIV analysis, as this can greatly help improve the accuracy of the PIV analysis. To make a comparison among cases easier, the time when the water level at the position of WG1 exceeded 0.5 cm was defined to be the start time for all the cases (i.e. at this moment t was defined to be 0.0 s).

2.3 Experimental results

2.3.1. Hydrodynamics

Figure 3 shows the time history of the water surface elevation recorded at at WG2, WG3 and WG5. As shown in the figure, at the offshore point (WG2) the front profile of the wave resembles a solitary wave (measured time history at WG2 is compared with the theoretical results of Munk, 1949), but with an elongated tail. The waves underwent shoaling while traveling over the slope (WG4), broke between WG4 and WG5, and propagated over land as a bore. Dividing the distance between WG4 and WG5 by the time required for the wave crest to pass through them, the offshore wave propagation velocity near the shoreline was calculated to be 1.75 m/s (following the approach described in Takabatake et al., 2020a, though it should be noted that this is just the wave propagation velocity near the shoreline, and the bulk of the wave behind it may have a slightly different velocity). Since the scale of the present experiment was 1:80, the wave front velocity is estimated to be 15.7 m/s on the prototype scale (if Froude scaling law is applied). This resembles the offshore wave front velocity estimated near the shoreline (see Sanuki et al., 2013) for the *2011 Tohoku Earthquake Tsunami* (around 12 to 14 m/s). The same approach applied to WG5 and WG6 resulted in the onshore wave propagation velocity near the shoreline to be 2.22 m/s (19.9 m/s on the prototype scale). It should be noted that the generated wave had a relatively short wave period when compared to a real tsunami. Thus, the main focus of the present research is on the characteristics of a tsunami flow during the early stages of its impact, and not on the subsequent inundation flow. In addition, while two wave crests were recorded at WG5, only the effects of the first wave were investigated.

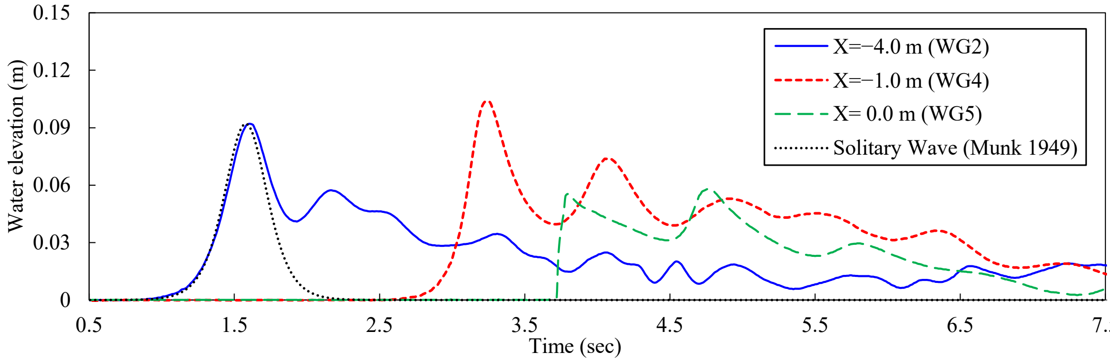

Figure 3 Time history of water elevation when no buildings are present. The blue line represents the time history at $x = -4.0$ m (WG2), the dotted red line represents the time history at $x = -1.0$ m (WG4), and the green line represents the time history at $x = 0.0$ m (WG5).

Figure 4 shows time history of flow depth, velocity, Froude number (F_r) and Reynolds number (R_e) recorded at x = 0.80 m without buildings. R_e and F_r were calculated using the recorded velocity (obtained from PIV analysis) and building width (0.10 m). Without buildings, the wave reached x = 0.80 m at around t = 4.0 s. The flow depth reached a maximum at around t = 4.2 s and remained at about the same value until t = 5.1 s. In contrast, the flow velocity reached its maximum value when the wave arrived at the reference point, and then gradually decreased. Relatively high F_r was recorded at the moment when the wave reached the reference point, due to the small flow depth at the front of the wave. Then, F_r gradually reduced but remained over 1.0 until t = 5.1 s, which means that the flow was supercritical. During a tsunami event, a high F_r of the inundation flow would only be observed near the coastline (though it should be noted that this would be heavily influenced by topography and the slope of the terrain and bed). In fact, Hayashi et al. (2013) estimated the F_r for the tsunami inundating the Sendai Plain during the *2011 Tohoku Earthquake and Tsunami*, and showed that F_r gradually decreased with distance from the coastline. Specifically, they demonstrated that while F_r was over 2.0 at 1,000 m from the coastline, it reduced to around 0.5 at 1,800 m. Thus, the results obtained can only be considered to be applicable to buildings situated in the vicinity of the coastline.

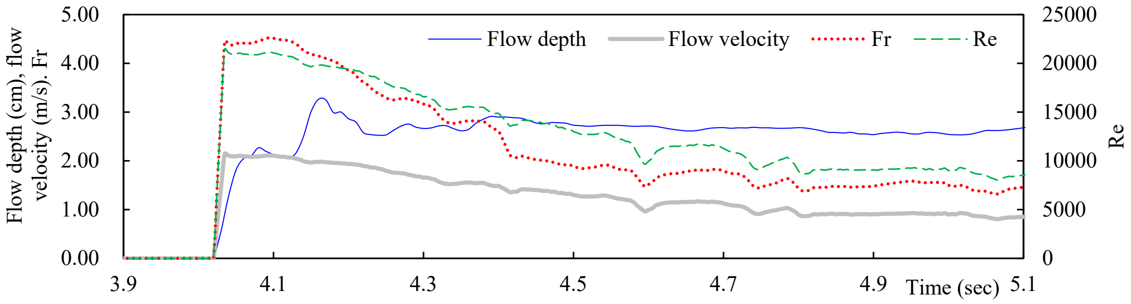

Figure 4 Time history of flow depth, velocity, Froude number (F_r) and Reynolds number (R_e) at x = 0.80 m for N0 case.

2.3.2. Observations

Figure 5 compares snapshots of the flow conditions taken using the high-speed camera for different building layouts. For the case of a single building, the flow was separated after the incident wave reached the building. The leeward (protected) area was gradually filled with water from both sides as the incident wave propagated landwards. When the separated flows collided behind the building, a hydraulic jump was generated due to the rapid increase in the depth of the flow (see **Figure 5a-iii**), evolving into a wake. Focusing on the front side of the building, the water surface raised immediately after the arrival of the wave (see **Figure 5a-i**), and a bow wave was subsequently generated. Then, a part of the bow wave propagated offshore, while the other part propagated in the direction of the stream, resulting in a complex water surface topography. The dashed red line in **Fig. 5a-iv** shows the position of the bow wave, implying that the depth of flow along this line is deeper than elsewhere.

Figures 5b and 5c show snapshots of the parallel layouts. **Figure 5b** shows the results for a gap of 5 cm (referred to as PA05, see **Table 1**) and **Figure 5c** shows the results for a gap of 30 cm (referred to as PA30). Comparing the front edge of the incoming tsunami between these two cases at t = 3.9 sec, the PA30 tsunami front reached further inland, especially behind the gap. This could be due to the greater blockage effect of PA05. At t = 4.1 sec, a slightly larger area was remained dry behind the buildings for PA30. After t = 4.3 sec, a hydraulic jump and its associated wake were observed in both cases. When focusing on the bow waves generated in front of each building, in the case of PA005, they merged at t = 4.3 sec into one large bow wave (see red line in **Figure 5b-iii**). In contrast, for a gap of 30 cm, the generated bow waves did not merge completely (see red line in **Figure 5c-iii**). As a result, in the case of PA30 a part of the bow wave propagated between the gap, generating strong turbulence behind it.

Figures 6a and 6b show snapshots for the perpendicular layouts. The general features of the flow were similar to those described for the single and parallel layouts. A bow wave was generated in front of the seaward building, and a wake was created behind the landward building. However, in the case of PE010 the rise in water level in front of the seaward building appears higher than in other cases (see the red line in **Figure 6a-iii**). This is probably due to the closer position of the landward building, which may have prevented the separated flows from merging behind the seaward building. A more complicated flow pattern was observed in the space between the obstacles. For instance, when an incoming wave entered the space of PE020, a hydraulic jump appeared behind the seaward obstacle, but a bow wave also occurred in front of the landward obstacle (see **Figure 6b-iv**).

Finally, it is worth noting that in the early stages of tsunami inundation the space immediately behind the buildings was kept dry, regardless of the layout (as shown in the area surrounded by dotted yellow lines).

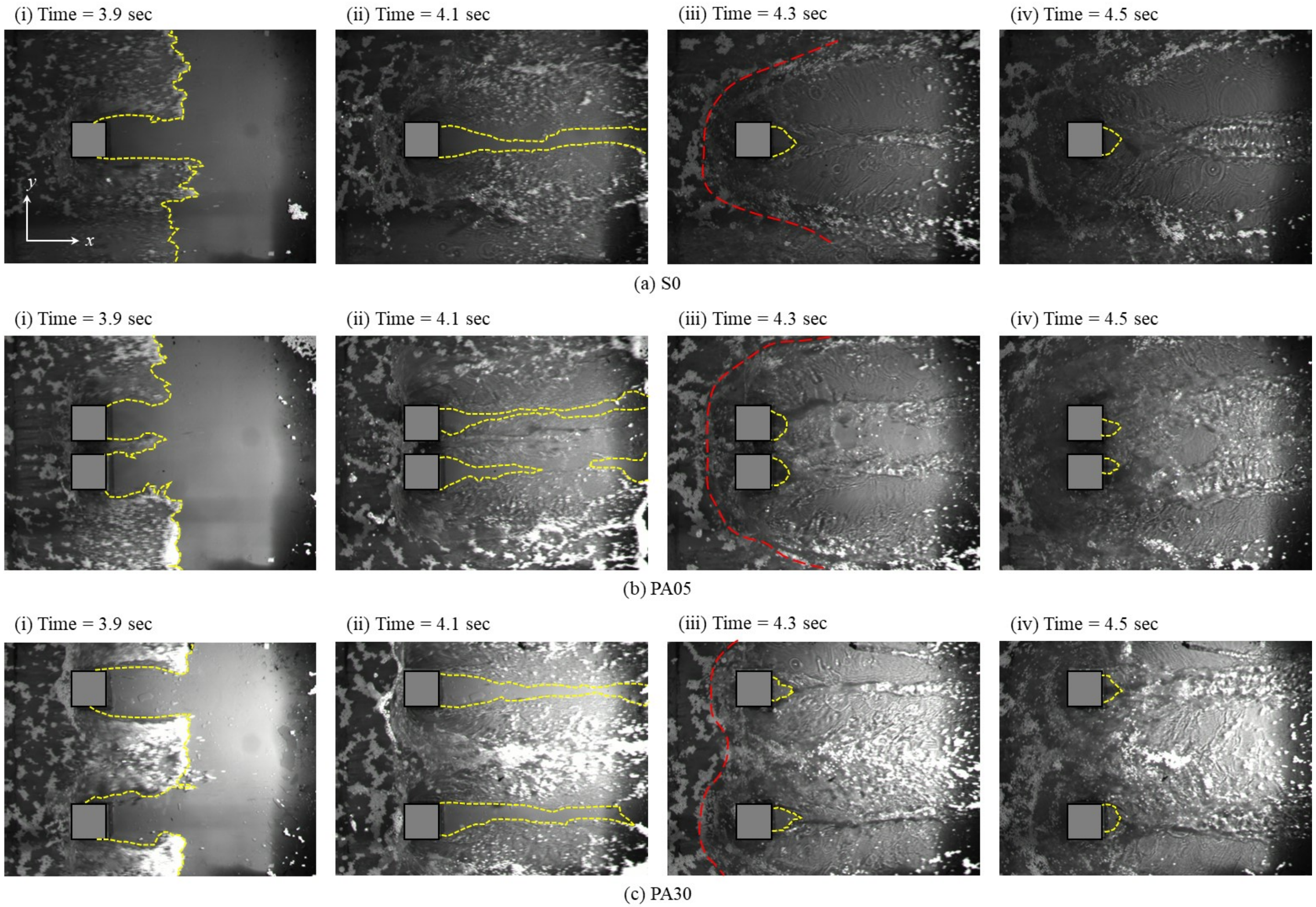

Figure 5 Snapshots of flow condition taken with the high-speed camera for (a) single layout, (b and c) parallel layouts (gap=5 cm, 30 cm). Dotted yellow lines indicate the boundary between wet and dry areas. Dashed red lines indicate the location of bow waves at $t = 4.3$ sec.

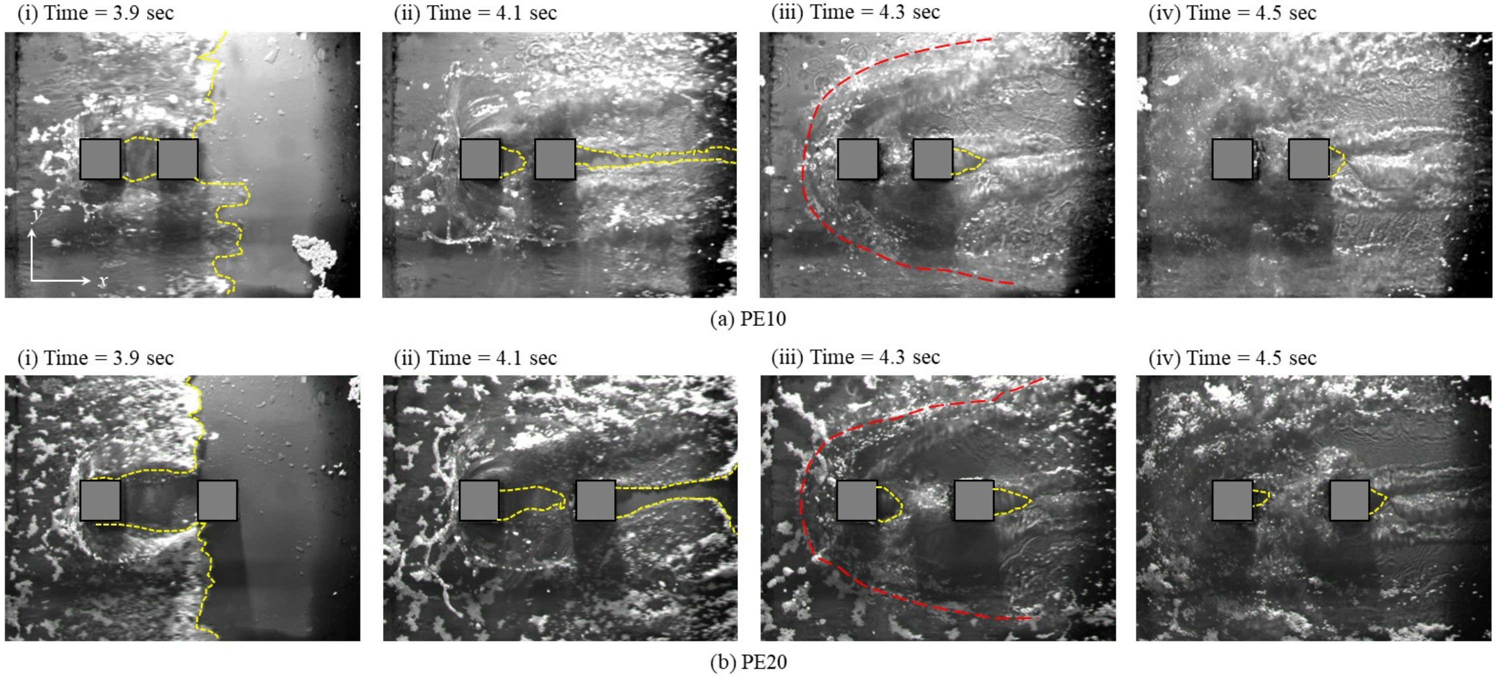

Figure 6 Snapshots of flow condition taken with the high-speed camera for (a and b) perpendicular layouts (gap = 10 cm, 20 cm). Dotted yellow lines indicate the boundary between wet and dry areas. Dashed red lines indicate the location of bow waves at t = 4.3 sec.

2.3.3. Velocity field

Figure 7 shows the spatial distribution of flow velocity averaged over t = 4.25–4.50 s (the time during which the wave front was passing through the target area), obtained through the surface PIV analysis (essentially meaning that the values correspond to the velocity of the water surface). The flow velocity was normalized over the value recorded in the absence of any buildings.

In all cases, the flow velocity in the area around x = 0.0 – 0.20 m decreased significantly. Although the width of the building is only 0.10 m, the low-velocity zone is wider than it. In the S0 and PE05 cases, over 40% lower velocities were observed from y = -0.15 m to y = 0.15 m (at x = 0.0 – 0.20 m), which corresponds to three times the width of the building. In the leeward side of the building, areas with significantly lower velocity were also found. In the single case, the flow velocities at x = 0.30 – 0.40 m and y = 0.0 m decreased by more than 70% compared to those recorded without the building (see **Figure 7a**).

In the parallel layout, the velocity in front of and behind the buildings decreased, but that behind the gap increased by about 10-30% (x = 0.40 – 0.80 m). Despite the flow contraction, the velocity between the buildings (x = 0.20 – 0.30 m) was less than that in the case without the buildings. This is probably due to the increased depth of flow and the fact that PIV only measures the velocity at the surface (and that near the bottom of the channel could have been higher).

Focusing on the perpendicular layout, the authors found that for the PE20 layout the lower velocity areas spread widely in the space between the two buildings (see **Figure 7e**). Since hydraulic jumps and bow waves occur clearly in the case of PE20, it is considered that such abrupt changes in the flow greatly affect the flow conditions around the space between the two buildings. In contrast, around the seaward building in the PE05 layout, the flow velocity was shown to drop more significantly (see the area where x = 0.20 – 0.35 m).

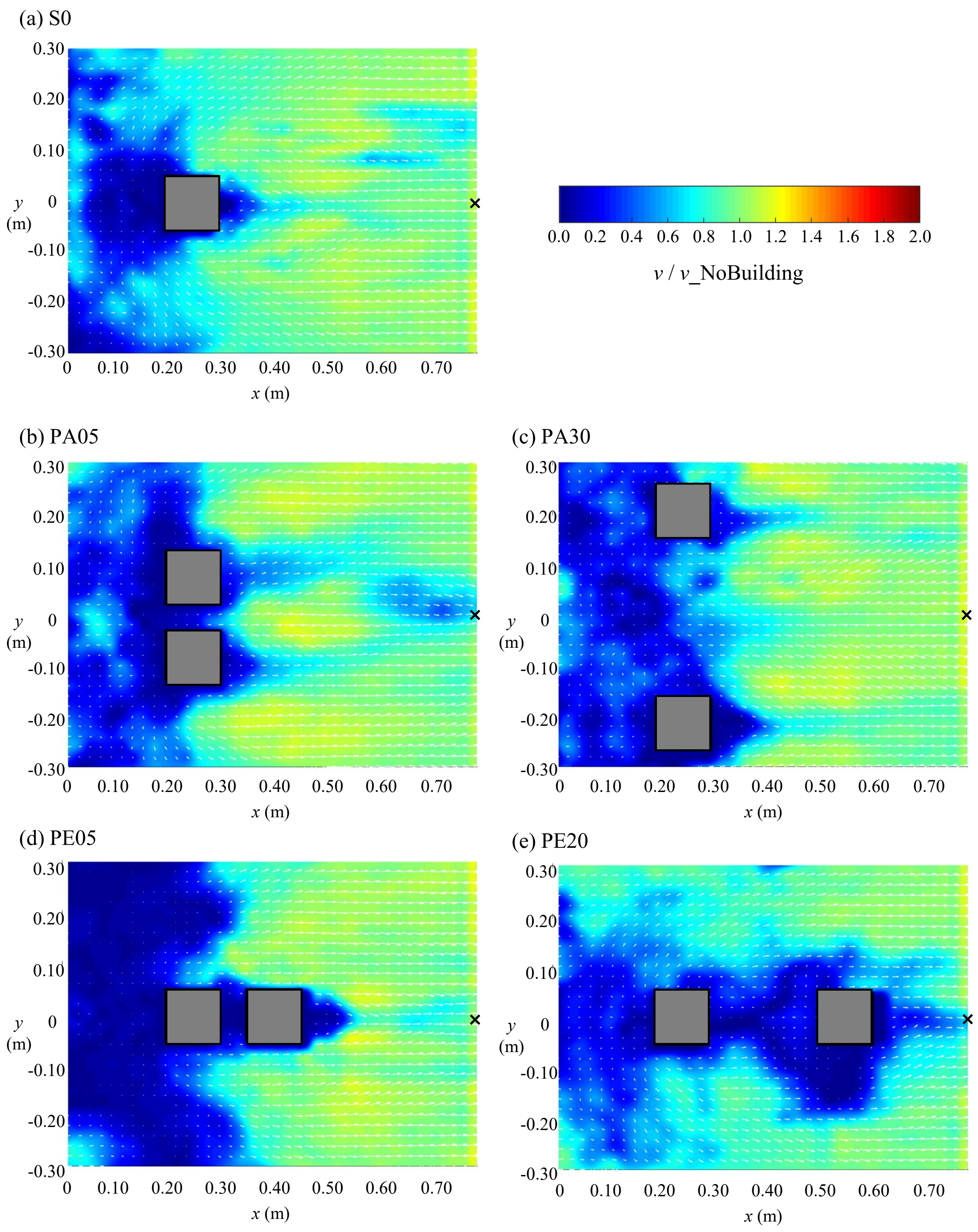

Figure 7 Normalized velocity field obtained from the surface PIV analysis for (a) single layout, (b and c) parallel layouts (gap = 5, 30 cm), and (d and e) perpendicular layouts (gap = 5, 20 cm). The values were normalized to the value recorded for the case without buildings and corresponds to the average value between $t = 4.25$ s and $t = 4.5$ s. The black cross in each image indicates the reference point.

2.3.4. Time history of flow depth, velocity, momentum flux at the reference point

Figure 8 shows the time history of flow depth, surface water velocity, and momentum flux at the reference point (x = 0.8 m, y = 0.0 m, see **Figure 7** for the location of this point) for the case with no buildings and a single building with a parallel layout gap of 0.05 m and 0.30 m. The momentum flux M_x in the flow direction is calculated by the following equation:

$$M_x = hv_x^2 \tag{1}$$

where h is the flow depth recorded by WG6, and v_x is the surface water velocity obtained from the PIV analysis at the same position of WG6 (in the x-direction). As explained earlier, in the case without buildings, while the flow depth value remained relatively constant, the velocity gradually decreased after the arrival of the wave. The maximum value of M_x appeared around t = 4.2 s, which corresponds to the time when the flow depth was maximum. In the S0 case, the incident wave reached the reference point at about t = 4.1 s. A relatively low M_x was recorded up until t = 4.3 s, since both the flow depth and velocity were smaller than when no building was present. In the PA05, the incident wave reached this point slightly earlier than for the S0, but the flow depth took longer to increase. As in this case the gap between the buildings is small, the incoming water mass cannot easily enter the space, leading to a slower increase in the flow depth behind the gap. Therefore, a relatively high surface water velocity was recorded with the arrival of the incident wave, but M_x remained low due to the small flow depth. In the PA30, the incoming wave was concentrated behind the gap, and thus the flow depth increased faster than in other cases. As both flow depth and velocity were maximized almost simultaneously, the maximum M_x was approximately 1.5 times that of the scenario without buildings.

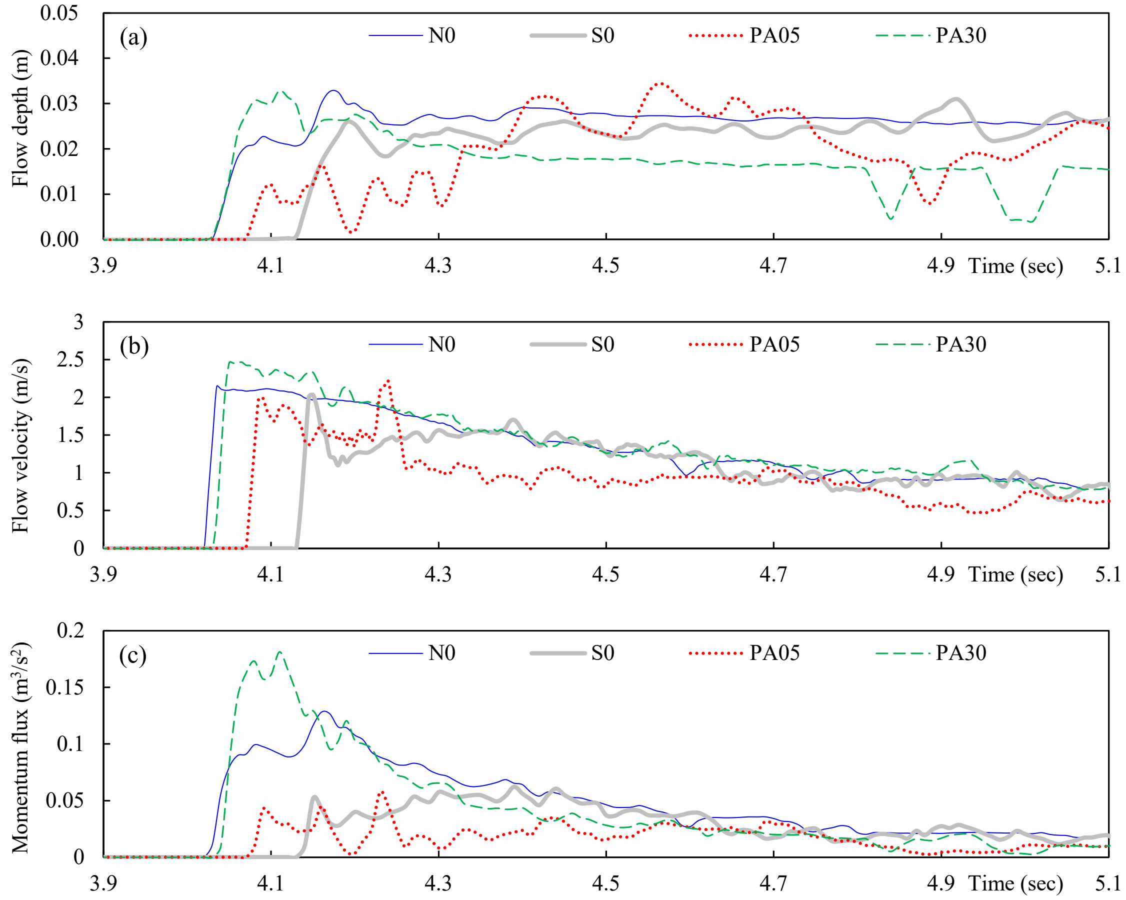

Figure 8 Time series plots of the experiment at the reference point for the no building, single, and parallel layouts: (a) flow depth, (b) surface water velocity, and (c) momentum flux. The blue line represents the case with no building, the thick grey line represents the single layout, the dotted red line represents a parallel layout with a gap = 0.05 m, and the dashed green line represents the parallel layout with a gap = 0.30 m.

Figure 9 shows the time history of flow depth, surface water velocity, and momentum flux at the reference point for the cases without buildings, a single building, and perpendicular layout with gaps of 0.05 m and 0.20 m. In general, the time history for PE05 and PE20 is similar to the time history for the single layout. However, after $t = 4.3$ s, the surface water velocity and M_x for PE20 became smaller than the others due to the shielding effect.

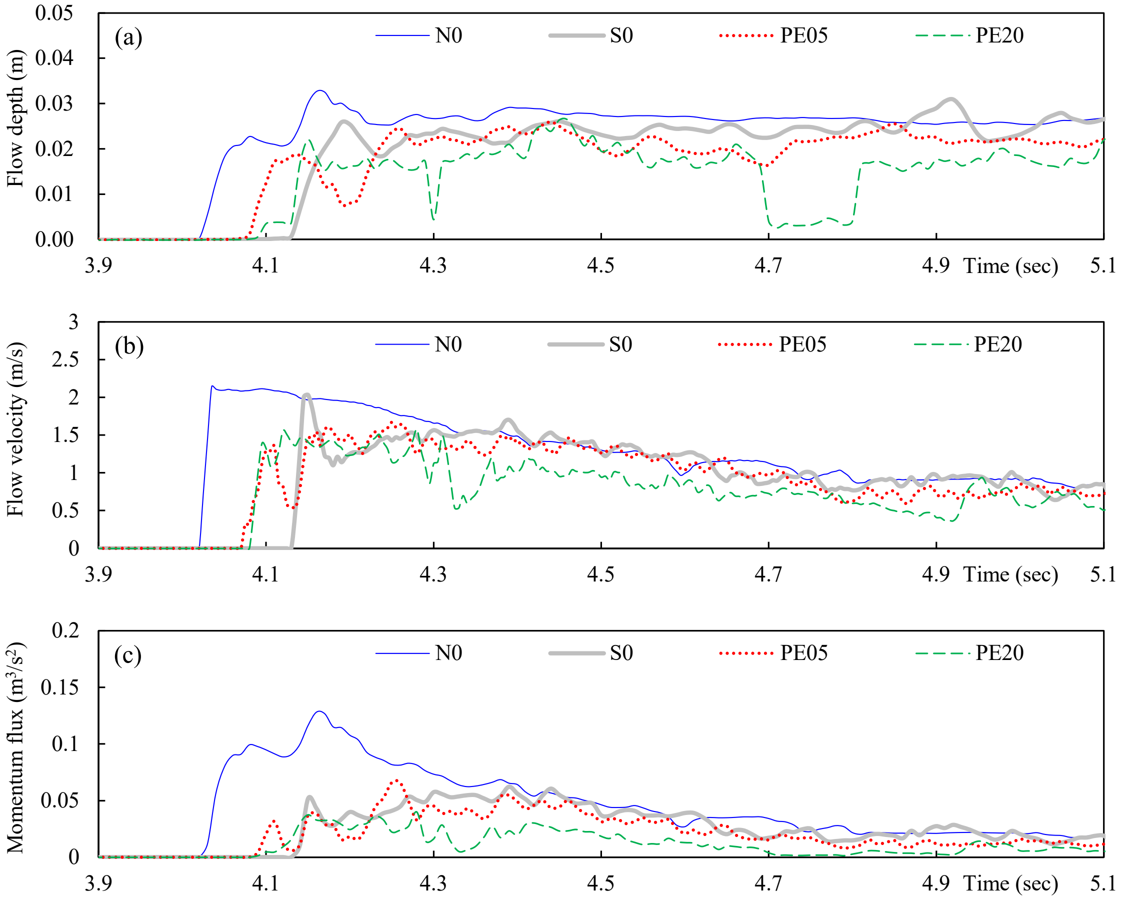

Figure 9 Time series plots of the experiment at the reference point for the no building, single and parallel layout cases; (a) flow depth, (b) surface water velocity and (c) momentum flux. The blue line represents the case with no buildings present, the grey thick line represents the single layout, the red dot line represents the perpendicular layout with a gap = 0.05 m and the green dash line represents the perpendicular layout with a gap = 0.20 m.

Figure 10 shows the maximum values of flow depth, velocity, and M_x recorded at the same reference point at the initial stage of the tsunami inundation (until t = 5.1 s). Again, the authors normalized the values to those recorded in the absence of buildings. In the single and perpendicular layouts, all values were smaller than in the case without building. In contrast, in the parallel layout, although the maximum surface water velocity was always slightly higher, the maximum flow depths of PA10 and PA20 were lower. There are clearer trends in the maximum momentum fluxes that depend on the size of the gap. For perpendicular layouts, as the gap size is larger, the maximum M_x became smaller. However, for the parallel layouts a higher maximum M_x was recorded as the gap size increased. The maximum M_x for PA05 was almost 40% smaller than for the case without buildings, but it was higher for PA30 by about 140%. This suggests that tsunami loads on a building behind a gap created by two buildings could be significantly affected by the size of this opening.

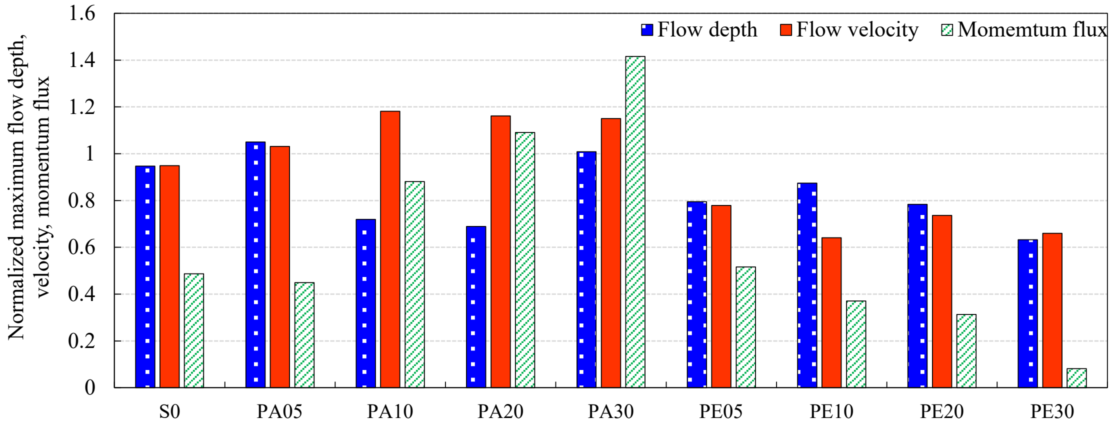

Figure 10 Maximum flow depth, velocity, and momentum flux recorded at the reference point during the initial stage of the tsunami inundation (until t = 5.1 s). The values were normalized to those recorded for the case without buildings.

3. Numerical Analysis

3.1. OpenFOAM

The experimental results show that the arrangement of buildings would significantly influence the flow features around and behind them. To deepen the understanding of the flow characteristics, the authors performed numerical simulations that focused on the shadowed area behind the buildings.

OpenFOAM (Open source Fields Operation and Manipulation, version 2.4.0) was used for the present numerical analysis. From the various solvers available in OpenFOAM, the authors chose the solver referred to as “interFoam”, which can simulate a two-phase flow separated by a free surface. A number of existing studies have utilized the solver and reported to have had succeeded in reproducing a tsunami-like wave recorded in laboratory experiments (e.g. Douglas et al., 2015; Oda et al., 2014; Iimura et al., 2020; Sarjamee et al., 2014). The governing equations used in the interFoam solver are the continuity equation (Eq.1) and the Navier-Stokes equation for incompressible flows (Eq.2).

$$\nabla \cdot \boldsymbol{U} = 0 \tag{1}$$

$$\frac{\partial \rho \boldsymbol{U}}{\partial t} + \nabla \cdot (\rho \boldsymbol{U}\boldsymbol{U}) = -\nabla p^* + \nabla \cdot \boldsymbol{\tau} + \rho \boldsymbol{g} + f_s \quad (2)$$

where $\boldsymbol{U}$ is the velocity vector, ρ is the fluid density, t is the time, p^* is the pseudodynamic pressure, $\boldsymbol{\tau}$ is the viscous stress tensor, $\boldsymbol{g}$ is the gravitational acceleration vector, and f_s is the body force corresponding to the surface tension. In the interFoam solver these equations are discretized by the finite volume method, and then solved using the Pressure Implicit with Splitting of Operators (PISO) method (Issa, 1986). The free surface movement is tracked based on the technique of the Volume of Fluid (VOF) as shown in Eq.3 and 4.

$$\frac{\partial \alpha}{\partial t} + \nabla \cdot \boldsymbol{U}\alpha + \nabla \cdot \boldsymbol{U_c}\alpha(1-\alpha) = 0 \quad (3)$$

$$\rho = \alpha\rho_1 + (1-\alpha)\rho_2 \quad (4)$$

where $\boldsymbol{U_c}$ is defined as the compression velocity to control the excessive diffusion of the interface, α is the phase fraction indicating the proportion of a grid cell filled with fluid (i.e., α is equal to 1 when the cell is completely filled with water, and 0 when completely filled with air), and ρ_1 and ρ_2 are the density of water and air, respectively.

3.2. Numerical Conditions

The computational domain used for the simulation is enclosed by the dashed rectangle shown in **Figure 1**. Mesh cell sizes are 0.05-0.0125 m in the *x*-direction, 0.05–0.025 m in the *y*-direction, and 0.05–0.00625 m in the *z*-direction. Finer mesh sizes were used near the landward area and building models.

The time histories of water surface elevation (recorded by WG2, as shown in **Figure 1**) and velocities in *x* direction (recorded at 0.10 m and 0.05 m from the bottom of the wave basin by ECM1 and ECM2, respectively) were inputted into the offshore boundary ($x = -4.0$m) to reproduce the incident tsunami wave. The offshore boundary and upper boundary (located at $z = 0.80$ m) were treated as ‘patch’, which contains no geometric or topological information and is suitable for inlet and outlet faces. The bottom of the wave basin, landward area, and the surface of building models were treated as ‘wall’, and the velocity there was fixed as zero (no slip condition).

It is important to include a turbulence model to precisely simulate the complex fluid interactions. In the present study, among the various turbulence models implemented in OpenFOAM, the Spalart-Allmaras DDES (Delayed Detached Eddy Simulation) model was selected. The Spalart-Allmaras DDES is based on the technique of DES (Detached Eddy Simulation), in which both RANS (Reynolds Averaged Navier-Stokes) and LES (Large Eddy Simulation) methods are combined (more specifically, the flow near the wall is modelled by the RANS method, while the turbulence far from it is calculated by LES method) (see Squires, 2004 for further explanation). Iimura et al. (2020) reported that the Spalart-Allmaras DDES model is able to successfully reproduce a tsunami-like wave inundating over the land area of this experimental basin.

3.3. Validation of the numerical simulation

The authors first validated OpenFOAM to confirm that it can accurately replicate the experiments conducted. **Figure 11** compares the time history of simulated and experimental water surface elevation at offshore points, flow depth, and velocity at the reference point for the single layout case. Despite some minor inconsistencies, the OpenFOAM results are generally in good agreement with the experimental results. **Figure 12** shows the velocity distribution recorded at t = 4.25 s for the S0 and PA30, indicating that both high and low velocities were also well reproduced by the OpenFOAM simulations.

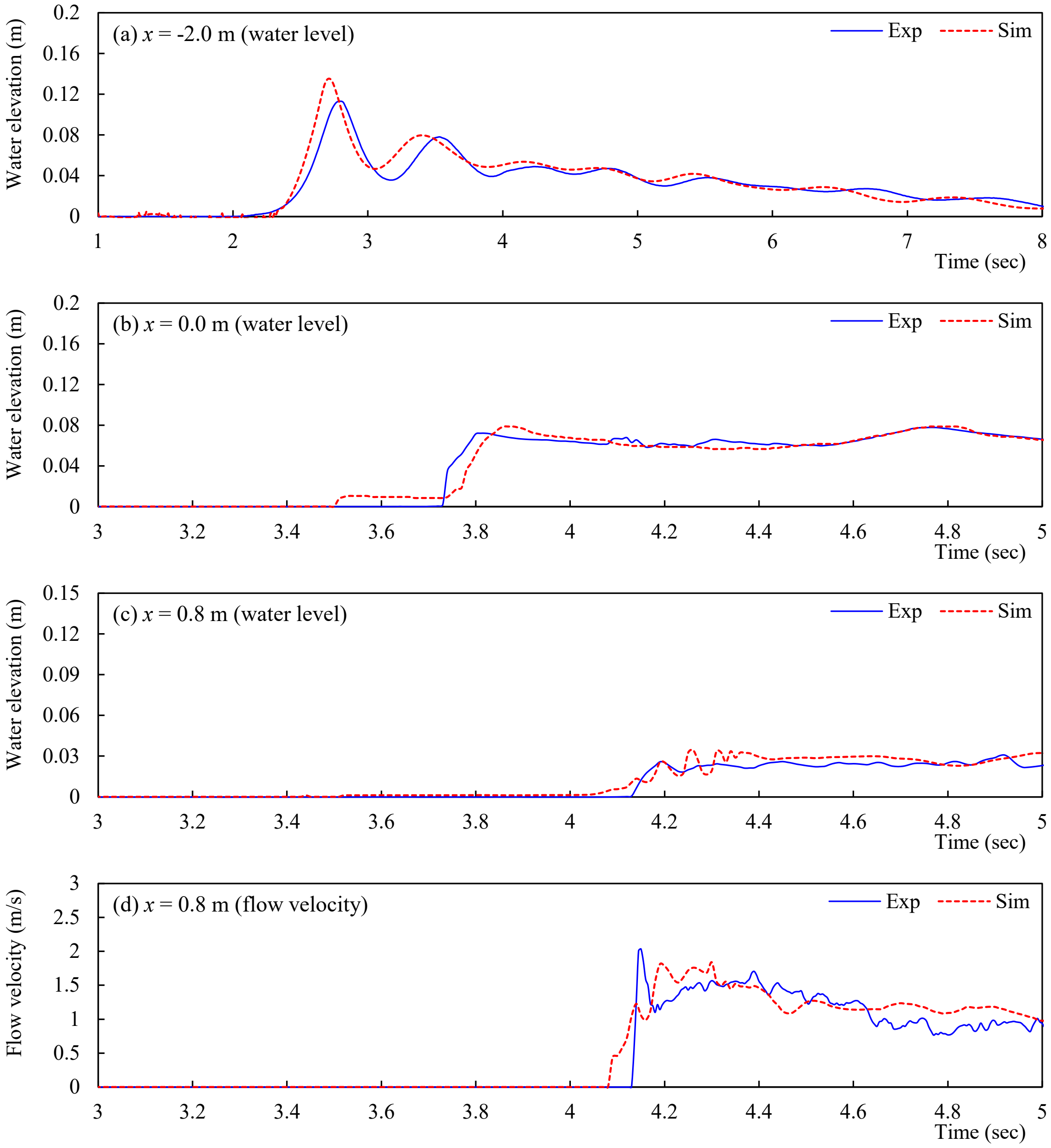

Figure 11 Comparison of simulated and experimental time histories for S0 case: (a) water surface elevation at $x = -4.0$ m, (b) water surface elevation at $x = 0.0$ m, (c) water surface elevation at $x = 0.8$ m, and (d) surface water velocity at $x = 0.8$ m.

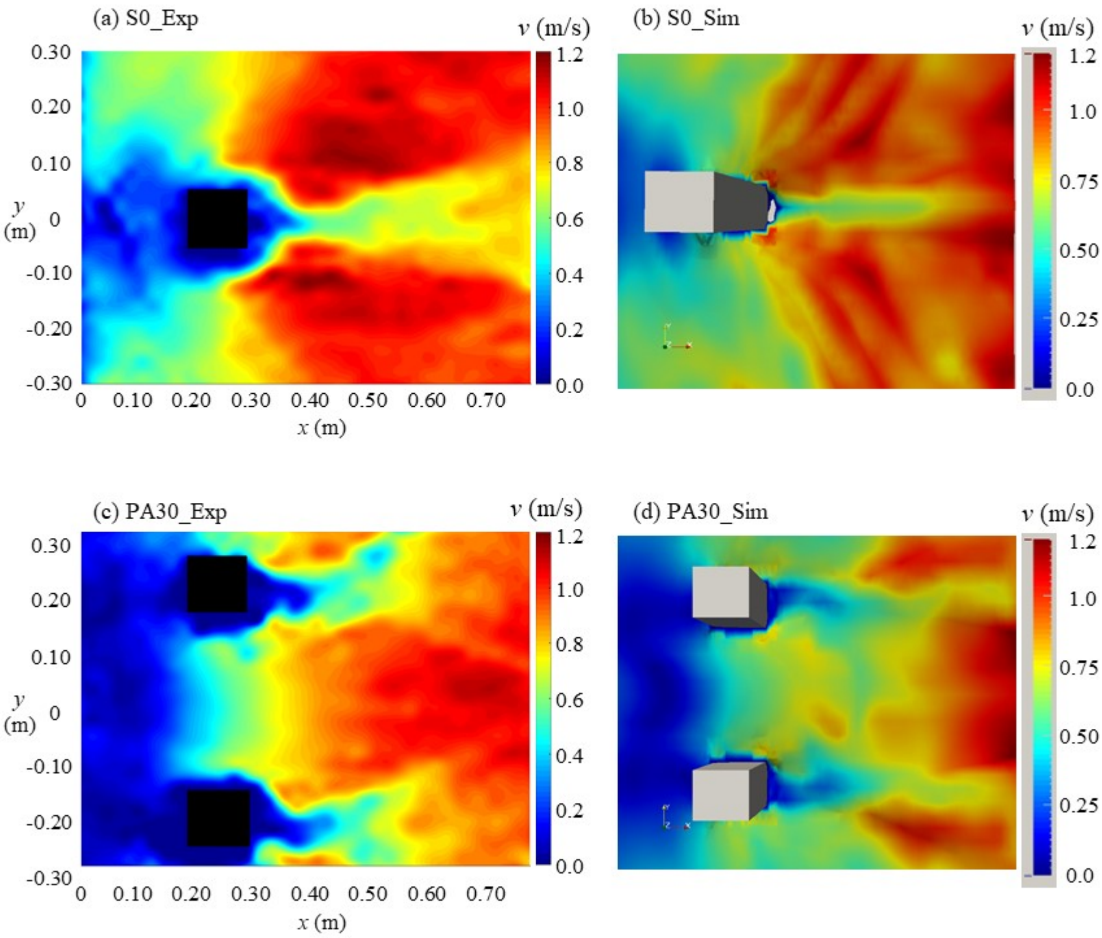

Figure 12 Comparison of simulated and experimental velocity distribution recorded at t = 4.25 s. For S0: (a) experiment and (b) simulation, and for PA30: (c) experiment and (d) simulation.

Figure 13 compares the maximum flow depth and surface water velocity at the reference point, showing a good agreement between the experiments and the OpenFOAM simulations (differences between them were within 30%, except for PA030).

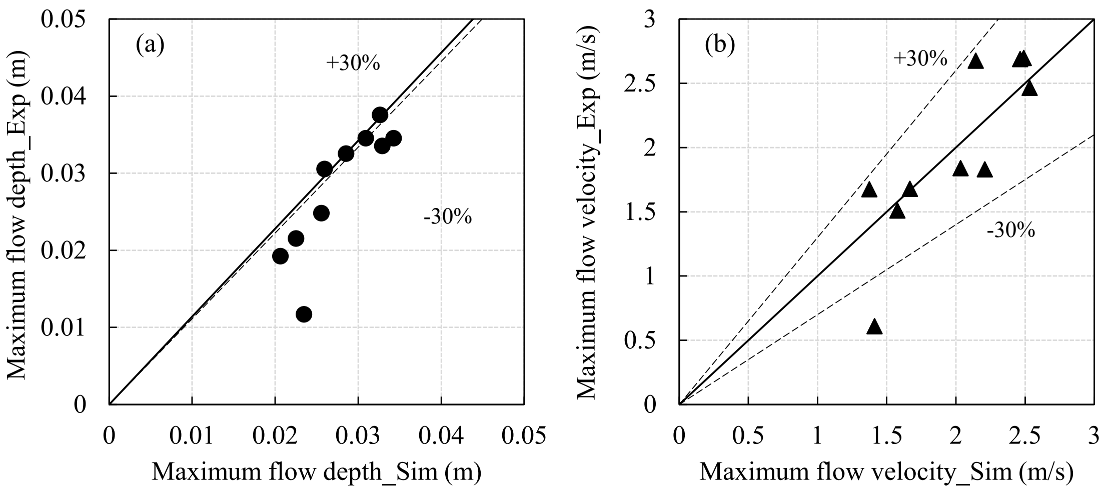

Figure 13. Comparison between simulated and experimental maximum values. (a) Flow depth, (b) surface water velocity.

3.4. Flow characteristics in the leeward area of the buildings

Figures 14 and **15** show maximum flow depths and cross-sectional averaged velocities (x-direction) simulated along the centreline of the building during the passage of the wave (for parallel layouts, the maximum values of the two buildings were averaged). In both figures, the position of the building is indicated by thick grey lines. For comparison, the results of the case without buildings are also shown.

In the S0, the flow depth in front of the building rose to about three times that without a building. The flow depth was also shown to be significantly lower behind the building. However, at $x > 0.70$ m the flow depth returned to the same value as that of the N0 case (**Figure 14**). Near-zero velocity was simulated on the leeside of the building, which gradually increased with distance. However, the velocity did not reach the level of that where no building was present (**Figure 14**). In all parallel layouts the flow depth and velocity became similar to that of the single layout, indicating that the presence of other neighbouring buildings does not significantly affect the flow field along the centreline of each building (see **Figure 14a** and **Figure 15a**).

Focusing on the results of perpendicular layout, both the flow depth and velocity behind the landward building were significantly lower than the single layout. Notably, in the area within about 0.10 m behind the landward building, significantly lower flow depths and velocities were simulated. Focusing on the space between the seaward and the landward buildings, the flow depth became deeper due to the presence of the landward building in all cases. In particular, in the case of PE20 and PE30, the flow depths increased rapidly in the immediate vicinity of the landward building, reaching about 50% of the simulated flow depth in front of the seaward building. However, the simulated maximum velocities were small, near zero in the PE05 and PE10 spaces, but approached that of the single layout in the other two cases. The results suggest that the shielding effect becomes more pronounced in the lee side of the building.

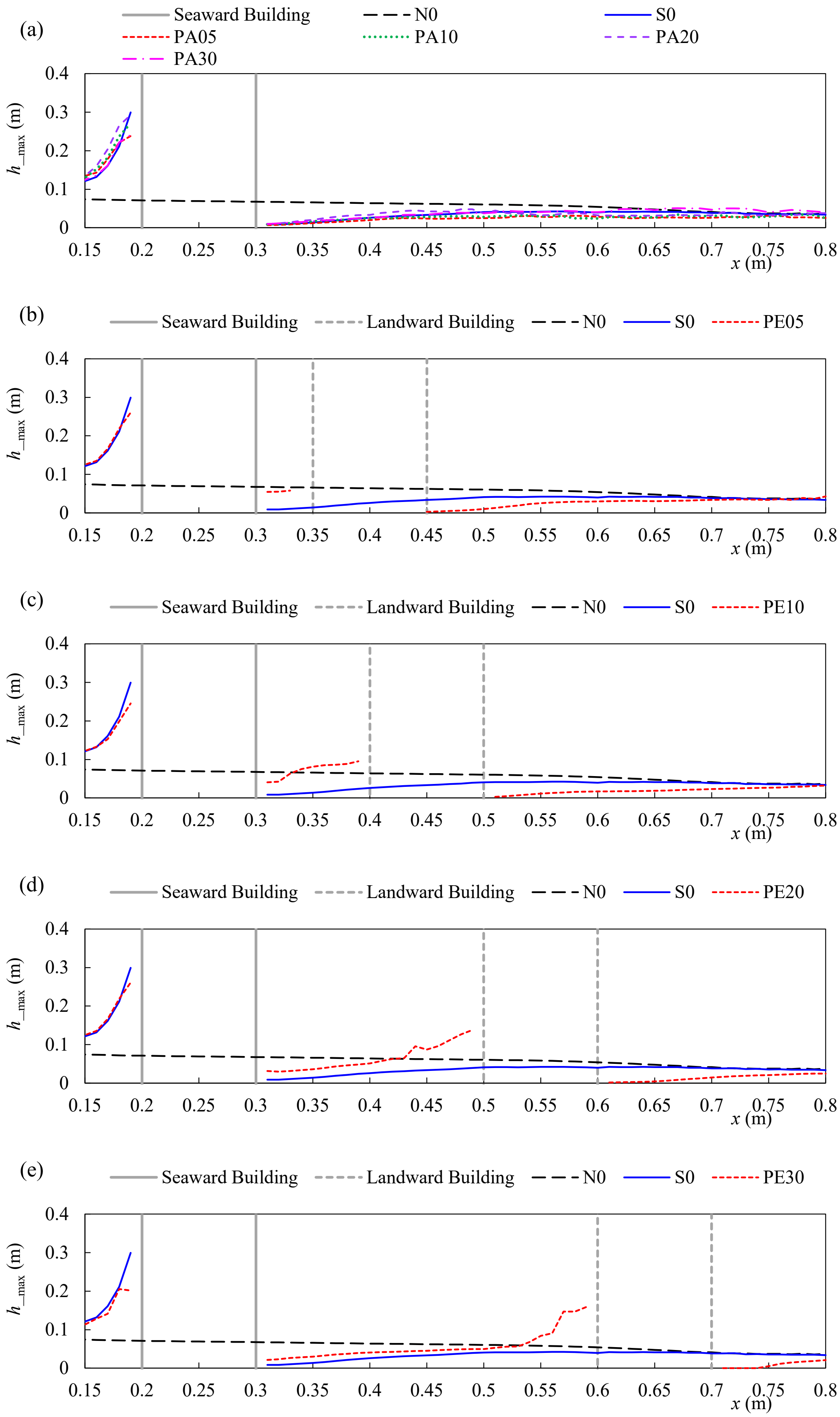

Figure 14 Spatial distribution of maximum flow depth along the centreline of building/s. The results where no buildings are present and single cases are shown against the cases of (a) Parallel, (b) PE05, (c) PE10, (d) PE20, and (e) PE30.

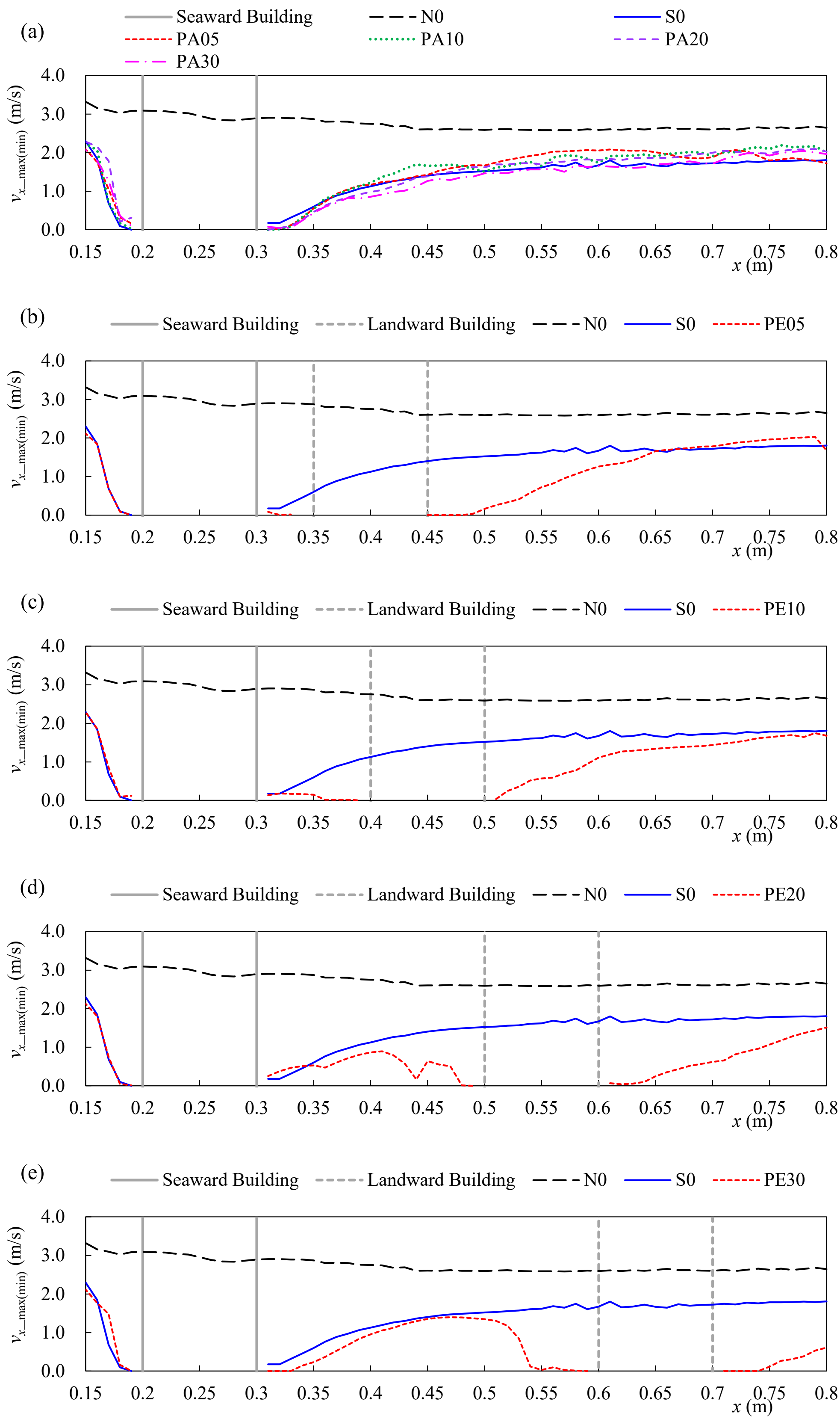

Figure 15 Spatial distribution of maximum (or minimum) flow velocity in x direction along the centerline of building(s). The results of N0 and S0 cases are shown together with the cases of (a) Parallel, (b) PE05, (c) PE10, (d) PE20, and (e) PE30.

4. Discussion

Video shots taken with a high-speed camera and subsequent PIV analysis revealed that the flow field of the wave during its passage was significantly changed according to the layout of the buildings. Notably, the PIV analysis revealed that the flow velocity decreased by more than 40% over a relatively large area (at least three times wider than the building width for the single and perpendicular layout cases) in front of the building(s), regardless of the building layout. Several researchers have investigated the effects of seaward obstacles on building situated behind them (Nouri et al. 2010; Weller et al. 2020). In that sense, it is interesting for future research to focus on the impacts of landward obstacles on buildings situated in front of them. As shown in this study, the flow field changed significantly in front of the buildings. Thus the direction of the overturning moment acting on the buildings situated in front of the landward obstacles and local pressures exerted on its structural elements would be changed.

Experimental results showed that all flow depths, velocities, and momentum fluxes at a given point are also sensitive to the layout of the buildings. No wave loadings on any of the structures were recorded in this experiment, but the results of momentum flux suggest that these should be significantly affected as well. While conducting a direct comparison is difficult, it would be meaningful to investigate the results obtained for the maximum momentum flux in light of the latest design standards for tsunami loading. The ASCE 7-16 Chapter C6 describes how to calculate the effects of the blockage ratio on a tsunami load. One of the methods, based on Nouri et al. (2010), suggests a force increase ratio with respect to a blockage ratio (BR), defined as $1-W_c/W$, where W is the channel width, and W_c is the constricted width. Another method, based on Thomas et al. (2015), expresses the force increase ratio using the wake clearance angle β. Both methods indicate that if the gap between the offshore buildings is sufficiently large ($0 < \mathrm{BR} < 0.25$, $\beta > 35°$), the rate of force increase becomes linearly larger with decreasing the gap (i.e., the channeling effect amplifies the force). In contrast, if the gap is relatively small ($\mathrm{BR} > 0.25$, $\beta < 20°$), it decreases linearly as the gap decreases (i.e., the flow is redirected due to the small gap, instead of concentrating through it). The blockage rate and wake clearance angles in the present experiments are BR=0.80, β=2.4° (PA05), BR=0.67, β=4.8° (PA10), BR=0.50, β=9.5° (PA20), and BR=0.40, β=14.0° (PA30). This means that the current experiments were all conducted in the relatively small gap region, with the results agreeing well with those of Thomas et al. (2016), as the normalized maximum flux also decreases linearly as the gap decreases. Therefore, the present works support to some extent the validity of the methods proposed in ASCE 7-16.

The obtained flow velocity at the reference point can also be compared with the results in Nouri et al. (2010). The results of these authors' velocity amplification ratio, defined as the ratio of maximum flow velocity in a given case to that where no obstacle is present is shown in **Figure 16,** along with the current experimental results. The ratios of BR=0.375 and BR=0.425 in Nouri et al. (2010) are always smaller than 1.0, but the current results are about 1.2 even for higher BR values. Current experiments were performed in a 3D basin, so the incoming wave was not influenced by the sidewalls of the channel. Thus, the fact that this ratio does not decrease even when BR increases suggests that 2D experiments probably underestimate the velocity amplification factors, highlighting the importance of performing such experiments in a 3D basin. As velocity amplification factor would also depend on the F_r, it is meaningful to investigate such effects.

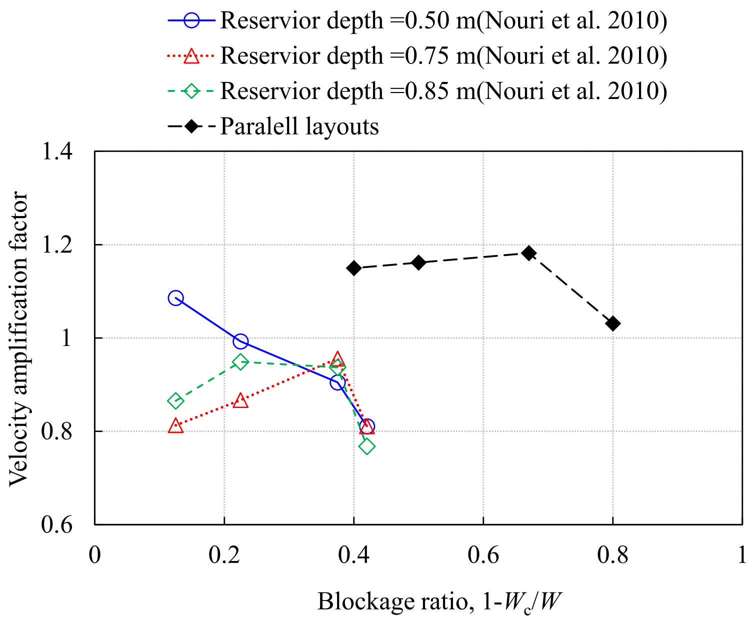

Figure 16 Comparison of velocity amplification factor between Nouri et al. (2010) and the current experiments. In Nouri et al. (2010), the depth in the reservoir was changed to generate different tsunami heights.

Both experimental and simulation results showed that areas where the flow depth and velocity were significantly reduced appeared within 0.10 m (equivalent to the width of the building) from the leeside of the building. This finding can be used in the design of evacuation buildings, which could be placed right behind a sturdy structure (ideally built with reinforced concrete) to lower their costs and/or make them safer (by receiving lower tsunami loads). The importance of increasing the number of available evacuation buildings has been reported elsewhere in literature (Takabatake et al. 2020b-d; Jiang and Murao 2017). Especially, if a coastal area is a well-known sightseeing destination or a popular beach, the number of evacuees would likely exceed the total capacity of evacuation buildings during summer periods (Takabatake et al. 2017, 2018), emphasizing the need to increase the number of available evacuation buildings.

Despite the findings above further research is clearly needed on this topic, considering many of the limitations of this study. Basically, the effect of the building layout on tsunami run-up flow can depend on the shape of the generated wave (such as nonbreaking and breaking; only breaking waves were used in this study) and building shape (such as size and angle with regards to the flow direction). The hydrodynamic forcing condition used in this study was an elongated solitary wave. Solitary waves have been used in several studies investigating wave forces on structures, debris transport, and wave propagation. The issues with the wave duration (Madsen et al., 2008) are well-known, though recent studies into impulse waves generated from landslides and ice calving (Heller et al., 2019) have similar properties to solitary waves. Additionally, throughout the results, the present study is compared with different wave conditions including a broken and unbroken error function wave (Winter et al., 2020) and dam-break wave (Nouri et al., 2010). Baldock et al. (2012) noted that broken solitary waves over a horizontal slope can be approximately modelled using a dam-break wave, though with a significantly reduced period. Considering the limitations of the elongated solitary wave, it can be assumed that these experiments predominantly would model the incipient hydrodynamics of a tsunami wave.

Tsunamis having different F_r would also produce different results from the present study. Therefore, it is important to increase the number of experimental cases by changing the shape of the "tsunami wave", associated with a variety of F_r, and the size and angle of the building models. When performing hydraulic experiments with Froude similitude, maintaining a high R_e is known to be important (Goseberg et al., 2015). For instance, based on overtopping experiments, Schüttrumpf (2001) recommended R_e to be greater than 10^3. Although the R_e in the present experiment exceeds this value, it does not reach the value of 1.00×10^6 (as shown in **Figure 4**) which would be a typical value for an actual tsunami in the field (Bricker et al., 2015). Thus, the vortices around the buildings may not be adequately modelled in the present experiments. To overcome such scaling effects and reproduce the vortices more correctly, it would be important to perform experiments in a larger scale. Combining these factors with various types of building layouts would help to improve the understanding of the inundation flow that takes place during a tsunami. Furthermore, conducting additional numerical simulations to further clarify the effects of building layouts on the tsunami-run-up flow could prove to be effective, given that the present work has validated the use of OpenFOAM for such studies.

5. Conclusions

The purpose of this study was to investigate how different layouts of buildings affect 1) the tsunami inundation process and spatial velocity distribution, 2) the flow depth and velocity at a specific point, and 3) the extent of the area where shielding effects take place. A total of nine different building layouts were investigated, both experimentally and numerically.

High-speed video footage and subsequent PIV analysis showed significant differences in the behaviour of the wave run-up flow among different building layouts. However, the PIV analysis also revealed a decrease in the flow velocity in front of and immediately behind the building(s), regardless of their layout. In front of the building(s), the velocity decreased by 40% throughout an area at least three times the width of the building (perpendicular to the direction of wave propagation). This suggests the need to focus more on the effects of landward obstacles on structures situated in front of them. It was also shown that the recorded time history of flow depth, velocity, and momentum flux significantly varies among the different building layouts. The current results with parallel layouts supports the validity of the method for calculating the channeling effects of tsunami loads according to ASCE 7-16. However, since the observed velocity amplification was different from that reported in experiments using 2D flume results (Nouri et al. 2010), additional experiments using 3D wave basins are necessary to further clarify the impacts of building layouts.

The present experiments and simulations show that areas where the flow depth and velocity drop significantly appear within 0.10 m (equivalent to the width of the building) from the leeside of the building. The findings are especially useful in areas where additional evacuation buildings are needed, as constructing them directly behind another study structure could reduce construction costs and increase their stability. However, it is essential to perform additional experiments and simulations using a variety of incident tsunamis, sizes, and angles of the building. Other aspects, such as coastal structures, accumulated debris, and changes in the channel slope, also need to be considered to support the findings obtained from this study.

Acknowledgements

The present work was performed as a part of the activities of the Research Institute of Sustainable Future Society, Waseda Research Institute for Science and Engineering, Waseda University.

References:

ASCE. 2017. *Minimum Design Loads and Associated Criteria for Buildings and Other Structures: ASCE/SEI 7–16*. Virgina, USA: American Society of Civil Engineers.

Bricker, J. D., Gibson, S., Takagi, H., and Imamura, F. 2015. "On the need for larger manning's roughness coefficients in depth-integrated tsunami inundation models." *Coastal Engineering Journal* 57(2): 1550005. doi:10.1142/S0578563415500059.

Cox, D. T., Tomita, T., Lynett, P. J., and Holman. R. 2008. "Tsunami inundation with macroroughness in the constructed environment." *Coastal Engineering Proceedings* 1(31): 1421–1432. doi:10.1142/9789814277426_0118

Dalrymple, R. A., and Kriebel, D. L. 2005. "Lessons in engineering from the tsunami in Thailand." *The Bridge, Nat. Acad. Eng.* 35(2): 4–16.

Douglas, S., and Nistor, I. 2015. "On the effect of bed condition on the development of tsunami-induced loading on structures using OpenFOAM." *Natural Hazards* 76: 1335–1356. doi:10.1007/s11069-014-1552-2.

Esteban, M., Glasbergen, T., Takabatake, T., Hofland, B., Nishizaki, S., Nishida, Y., Stolle, J., et al. 2017. "Overtopping of coastal structures by tsunami waves." *Geosciences* 7: 121. doi:10.3390/geosciences7040121.

Esteban, M., Roubos, J. J., Iimura, K., Salet, J. T., Hofland, B., Bricker, J. D., Ishii, H., et al. 2020. "Effect of bed roughness on tsunami bore propagation and overtopping." *Coastal Engineering* 157: 103539. doi:10.1016/j.coastaleng.2019.103539.

Goseberg, N., Bremm, G., Schlurmann, T. and Nistor, I. 2015. "A Transient approach flow acting on a square cylinder - flow pattern and horizontal forces." *Proceedings of the 36th IAHR World Congress* 1–12.

Goseberg, N. 2013. "Reduction ofmaximum tsunami run-up due to the in- teraction with beachfront development—application of single sinusoidal waves." *Nat. Hazards Earth Syst. Sci.* 13(11): 2991–3010. doi:10.5194/nhess-13-2991-2013.

Goseberg, N., and Schlurmann, T. 2014. "Non-Stationary Flow Around Buildings During Run-Up of Tsunami Waves on a Plain Beach." *Coastal Engineering Proceedings* 1(34): 21. doi:10.9753/icce.v34.currents.21.

Harnantyari, A., Takabatake, T., Esteban, M., Valenzuela, P., Nishida, Y., Shibayama, T., Achiari, H., et al. 2020. "Tsunami awareness and evacuation behaviour during the 2018 Sulawesi Earthquake tsunami." *International Journal of Disaster Risk Reduction* 43: 101389. doi:10.1016/j.ijdrr.2019.101389

Hatzikyriakou, A., and Lin, N. 2017. "Impact of performance interdependencies on structural vulnerability: A systems perspective of storm surge risk to coastal residential communities." *Reliability Engineering & System Safety* 158: 106-116. https://doi.org/10.1016/j.ress.2016.10.011

Hayashi, S., and Koshimura, S. 2013. "The 2011 Tohoku tsunami flow velocity estimation by the aerial video analysis and numerical modeling." *Journal of Disaster Research* 8(4): 561–572.

Iimura, K, Shibayama, T., Takabatake, T., and Esteban, M. 2020. "Experimental and numerical investigation of tsunami behavior around two upright sea dikes with different heights." *Coastal Engineering Journal.* Accepted.

Issa, R. I. 1986. "Solution of the implicitly discretised fluid flow equations by operator-splitting." *Journal of Computational Physics* 62: 40–65. doi:10.1016/0021-9991(86)90099-9.

Jiang D. and O. Murao. 2017. "Consideration of tsunami risk reduction effect focusing on tourists' evacuation time in Katase-Nishihama and Kugenuma district, Fujisawa City." *Journal of Social Safety Science* 31: 117–124. doi: 10.11314/jisss.31.117.

Kakinuma, T., Tsujimoto, G., Yasuda, T., and Tamada, T., 2012. "Trace survey of the Tohoku tsunami in the north of Miyagi prefecture and numerical simulation of bidirectional tsunamis in Utatsusaki peninsula." *Journal of Japan Society of Civil Engineers, Ser. B2 (Coastal Engineering)* 68(2): I_361-I_365.

Nakamura, T., Nakashima, A., and Mizutani, N. 2014. "Three-dimensional numerical analysis of tsunami-induced wave force acting on an inland structure in the presence of nearshore structures." *Journal of Japan Society of Civil Engineers, Ser. B2 (Coastal Engineering)* 70(2): I_816-I_820. doi:10.2208/kaigan.70.I_816.

National Institute for Land and Infrastructure Management (NILIM) & Building Research Institute (BRI). 2012. "Report on field surveys and subsequent investigations of building damage following the 2011 off the Pacific coast of Tohoku

Earthquake." *TECHNICAL NOTE National Institute for Land and Infrastructure Management 674, Building Research Data 136* 6.4.1-6.4.23. https://www.kenken.go.jp/japanese/contents/topics/20110311/0311report.html. (Accessed 17 September 2020)

Mori, N., Takahashi, T., Yasuda, T., and Yanagisawa, H. 2011. "Survey of 2011 Tohoku earthquake tsunami inundation and run-up." *Geophysical Research Letters* 38(7): L00G14

Nouri, Y., Nistor, I., Palermo, D., and Cornett, A. 2010. "Experimental investigation of tsunami impact on free standing structures." *Coastal Engineering Journal* 52(1): 43–70. doi:10.1142 /S0578563410002117.

Oda, K., Okamoto, O., Miyazaki, K., and Sigiura, S. 2008. "Experiment on mitigation effects of on-land buildings." *Proceedings of Coastal Engineering, JSCE* 55: 1361–1365. doi:10.2208/proce1989.55.1361.

Oda, Y., Honda, T., and Takabatake, T. 2014. "Study on time series evaluation of tsunami force acting on land structures." *Journal of Japan Society of Civil Engineers, Ser. B2 (Coastal Engineering)* 70(2): I_796-I_800. doi:10.2208/kaigan.70.i_796.

Okamoto, O., Oda, K., Sugiura, S., Miyazaki, K., and Tanaka, S. 2009. "Experiment on mitigation effects of on-land buildings caused by tsunami and storm surges." *Journal of Japan Society of Civil Engineers, Ser. B2 (Coastal Engineering)* 65(1): 1361–1365. doi:10.2208/kaigan.65.1361.

Okumura, Y., Bando, N., Shikata, T., Yoneyama, N., and Kiyono, J. 2019. "Relathionship between building distribution and tsunami overtuning moment." *Journal of Japan Society of Civil Engineers, Ser. B2 (Coastal Engineering)* 75(1): I_861–I_876. doi:10.2208/kaigan.75.I_871

Park, H., Cox, D.T., Lynett, P. J., Wiebe, D. M., and Shin, S. 2013. "Tsunami inundation modeling in constructed environments: A physical and numerical comparison of free-surface elevation, velocity, and momentum flux." *Coastal Engineering* 79: 9–21. doi:10.1016/j .coastaleng.2013.04.002.

Prasetyo, A, Yasuda, T., Miyashita, T., and Mori, N. 2019. "Physical modeling and numerical analysis of tsunami inundation in a coastal city." *Frontiers in Built Environment* 5(46): 1-19. doi:10.3389/fbuil.2019.00046

Qin, X., Motley, M., LeVeque, R., Gonzalez, F., and Mueller, K. 2018a. "A comparison of a two-dimensional depth averaged flow model and a three-dimensional RANS model for predicting tsunami inundation and fluid forces." *Nat. Hazards Earth Syst. Sci.* 18: 2489–2506. doi:10.5194/nhess-2018-56.

Qin, X., Motley, M. R., and Marafi, N. A. 2018b. "Three-dimensional mod- eling oftsunami forces on coastal communities." *Coastal Engineering* 140: 43–59. doi:10.1016/j.coastaleng.2018.06.008.

Robertson, I., and Mohamed, A. 2009. "Development of performance based tsunami engineering, PBTE." *IABSE Symp. Rep.* 96(15): 16–23. doi:10.2749/222137809796068091.

Sanuki, H., Takemori, R., Tajima, Y., and Sato, S. 2013. "Study on tsunami flooding in river based on video images and numerical simulation." *Journal of Japan Society of Civil Engineers, Ser. B2 (Coastal Engineering)* 69(2): I_1296-I_1300. doi:10.2208/kaigan.69.i_196.

Sarjamee, S., Nistor, I., and Mohammadian, A. 2017. "Numerical investigation of the influence of extreme hydrodynamic forces on the geometry of structures using OpenFOAM." *Natural Hazards* 87(1): 213–35. doi:10.1007/s11069-017-2760-3.

Schüttrumpf, H. 2001. "Wellenüberlauf bei Seedeichen - Experimentelle und theoretische Untersuchungen." Braunschweig: Technical University Carolo-Wilhelmina.

Simamora, C., Shigihara, Y., and Fujima, K. 2007. "Experimental study on tsunami forces acting on structures." *Proceedings of Coastal Engineering, JSCE* 54: 831–835. doi:10.2208/proce1989.54.831.

Squires, K. D. 2004. "Detached-eddy simulation: current status and perspectives." *Proceedings of the fifth international ERCOFTAC Workshop on direct and large-eddy simulation* 465–480. doi:10.1007/978-1-4020-2313-2_49.

Stolle, J., Takabatake, T., Hamano, G., Ishii, H., Iimura, K., Shibayama, T., Nistor, I., Goseberg, N., and Petriu, E. 2019. "Debris transport over a sloped surface in tsunami-like flow conditions." *Coastal Engineering Journal* 61(2): 241–55. doi:10.1080/21664250.2019.1586288.

Stolle, J., Takabatake, T., Nistor, I., Mikami, T., Nishizaki, S., Hamano, G., Ishii, H., et al. 2018. "Experimental investigation of debris damming loads under transient supercritical flow conditions.” *Coastal Engineering* 139: 16–31. doi:j.coastaleng.2018.04.026.

Synolakis, C. E., and Kong, L. 2006. “Run up measurements of the December 2004 tsunami.” *Earthquake Spectra* 22(53): 567–591. https://doi.org/10.1098/rsta.2006.1824

Takabatake, T., Esteban, M., Nistor, I., Shibayama, T., and Nishizaki, S. 2020d. “Effectiveness of hard and soft tsunami countermeasures on loss of life under different population scenarios.” *International Journal of Disaster Risk Reduction* 45: 101491. doi:10.1016/j.ijdrr.2020.101491.

Takabatake, T., Fujisawa, K., Esteban, M., and Shibayama, T. 2020c. “Simulated effectiveness of a car evacuation from a tsunami.” *International Journal of Disaster Risk Reduction* 47: 101532. doi:10.1016/j.ijdrr.2020.101532.

Takabatake, T., Nistor, I., and St-Germain, P. 2020b. “Tsunami evacuation simulation for the District of Tofino, Vancouver Island, Canada.” *International Journal of Disaster Risk Reduction* 48: 101573. doi:10.1016/j.ijdrr.2020.101573.

Takabatake, T., Mäl, M., Han, D. C., Inagaki, N., Kishizaki, D., Esteban, M., and Shibayama, T. 2020a. “Physical modelling of tsunamis generated by subaerial, partially submerged and submarine landslide.” *Coastal Engineering Journal*. accepted.

Takabatake, T., Shibayama, T., Esteban, M., and Ishii, H. 2018. “Advanced casualty estimation based on tsunami evacuation intended behavior: case study at Yuigahama Beach, Kamakura, Japan.” *Natural Hazards* 92(3): 1763–1788. doi:10.1007/s11069-018-3277-0.

Takabatake, T., Shibayama, T., Esteban, M., Ishii, H., and Hamano, G. 2017. “Simulated tsunami evacuation behavior of local residents and visitors in Kamakura, Japan.” *International Journal of Disaster Risk Reduction* 23:1–14. doi:10.1016/j.ijdrr.2017.04.003.

Takabatake, T., Shibayama, T., Esteban, M., Achiari, H., Nurisman, N., Gelfi, M., Tarigan, T. A., et al. 2019. “Field survey and evacuation behaviour during the 2018 Sunda Strait Tsunami.” *Coastal Engineering Journal* 61(4): 423–443. doi:10.1080/21664250.2019.1647963

Thomas, S., Killian, J., and Bridges, K. J. 2015. “Influence of macroroughness on tsunami loading of coastal structures.” *J. Waterway, Port, Coastal, Ocean Eng.* 141(1): 04014028. doi:10.1061 /(ASCE)WW.1943-5460.0000268.

Tomiczek, T., Prasetyo, A., Mori, N., Yasuda, Y., and Kennedy, A. 2016. “Physical modelling of tsunami onshore propagation, peak pressures, and shielding effects in an urban building array.” *Coastal Engineering* 117: 97–112. doi:10.1016/j.coastaleng.2016.07.003.

Tomiczek, T., Prasetyo, A., Mori, N., Yasuda, T., and Kennedy, A. 2017. “Effects of a macro-roughness element on tsunami wave amplification, pressures, and loads: Physical model and comparison to Japanese and US design equations.” *Coastal Engineering Journal* 59 (1): 1750004-1–1750004-25. doi:10.1142/S0578563417500048.

Winter, A. O., Alam, M. S., Shekhar, K., Motley, M. R., Eberhard, M. O., Barbosa, A. R., Lomonaco, P., et al. 2020. “Tsunami-like wave forces on an elevated coastal structure: Effects of flow shielding and channeling.” *J. Waterway, Port, Coastal, Ocean Eng.* 146(4): 04020021. doi:10.1061/(ASCE)WW.1943-5460.0000581.

Wüthrich, D., Pfister, M., Nistor, I., & Schleiss, A. J. (2018). *“Experimental study on forces exerted on buildings with openings due to extreme hydrodynamic events”.* Coastal Engineering, 140, 72-86.